

# Hierarchical Toughening of Nacre-Like Composites

Madeleine Grossman, Dmitriy Pivovarov, Florian Bouville, Clemens Dransfeld, Kunal Masania,\* and André R. Studart\*

Reinforced polymer-based composites are attractive lightweight materials for aircrafts, automobiles, and turbine blades, but still show strength and fracture toughness lower than traditional metals. An interesting approach to address this issue is to fabricate composites with structural features that absorb part of the elastic energy stored in the material during fracture through extrinsic and intrinsic toughening mechanisms behind and ahead of the crack tip, respectively. Inspired by the nacreous layer of mollusk shells, the fracture behavior of multiscale composites that combine intrinsic toughness from a brick-and-mortar structure connected through nanoscale mineral bridges and extrinsic toughness arising from a brittle–ductile laminate architecture at the millimeter scale are fabricated and investigated. Such a hierarchical toughening approach increases the dissipated energy by more than 30-fold during fracture with minimal loss in stiffness and strength. Using simple energy balance arguments and fracture mechanics concepts, guidelines are established for the design of nacre-like composites with a remarkable combination of stiffness, strength, and toughness. This demonstrates the possibility to controllably introduce toughening mechanisms at different length scales and to thus fabricate hierarchical composites with high fracture resistance in spite of the brittle nature of their main inorganic constituents.

## 1. Introduction


Lightweight composites are increasingly important as structural materials for future sustainable transportation,<sup>[1]</sup> energy-harvesting,<sup>[2]</sup> and biomedical technologies.<sup>[3]</sup> A major goal in all these applications is to develop lightweight materials that combine enhanced stiffness with high strength and toughness. High strength and stiffness are required to enable the design of

structures that can bear mechanical loads without damage, whereas high toughness is essential for safety since it ensures a graceful, noncatastrophic failure of the material in case the strength is exceeded. A major challenge arises from the fact that strength and toughness are mutually exclusive in most synthetic materials.<sup>[4]</sup> This is because both properties are intrinsically related to the ability of chemical bonds to either resist or facilitate stress-induced deformation.<sup>[4]</sup> Thus, gains in toughness are normally accompanied by a reduction in strength and viceversa. Remarkably, many natural materials are able to overcome this general rule by combining both strength and toughness in hierarchical composite architectures. As a result of a long evolutionary process driven by the need of structural protection or attack, such biological materials achieve outstanding properties using ordinary and abundant building blocks.<sup>[5]</sup> Replicating, in synthetic composites, the strengthening and toughening strategies that have

evolved in these natural systems has been a major research goal in the field of bioinspired materials.<sup>[6]</sup> Such a research effort requires both understanding the design principles of biological materials and developing processing technologies that allow for their implementation in synthetic composites through bioinspired architectures with exquisite structural control.

Studying the structure and mechanical behavior of natural materials at multiple length scales has enabled a better understanding of the design principles underlying the combined strength and toughness of biological composites.<sup>[7]</sup> Strength and toughness is often reconciled by providing intrinsic and extrinsic toughening mechanisms at small and large length scales, respectively.<sup>[8]</sup> In bone, for instance, intrinsic toughening ahead of the crack tip arises from the relative sliding of mineralized collagen fibrils at sub-micrometer length scales. At larger length scales, in the range of 10s to 100s of microns, crack deflection and bridging caused by weak cement lines between bone lamella provide extrinsic mechanisms behind the crack tip that ensure an increasing resistance of the composite against crack growth.<sup>[9]</sup> In another prominent example, the nacreous layer of mollusk shells reaches intrinsic toughening by arranging inorganic platelets into a brick-and-mortar structure that is highly interconnected through mineral bridges, nanoasperities, and dovetailed and wavy features in a tough biopolymer matrix.<sup>[10]</sup> The strengthening effect arising from these nanoscale morphologies are combined with crack

Dr. M. Grossman, D. Pivovarov, Dr. F. Bouville, Dr. K. Masania, Prof. A. R. Studart  
Complex Materials  
Department of Materials  
ETH Zürich  
8093 Zürich, Switzerland  
E-mail: kunal.masania@mat.ethz.ch; andre.studart@mat.ethz.ch  
Prof. C. Dransfeld<sup>[†]</sup>  
Institute of Polymer Engineering  
FHNW University of Applied Sciences and Arts Northwestern  
Switzerland  
5210 Windisch, Switzerland

 The ORCID identification number(s) for the author(s) of this article can be found under <https://doi.org/10.1002/adfm.201806800>.

<sup>[†]</sup>Present address: Aerospace Manufacturing Technologies, Faculty of Aerospace Engineering, Delft University of Technology, Delft 2600 GB, The Netherlands

DOI: 10.1002/adfm.201806800

bridging, deflection, and platelet pull-out mechanisms at larger length scales to achieve very high toughness. Similar intrinsic and extrinsic mechanisms have been discovered and developed in synthetic materials such as metallic glasses,<sup>[11]</sup> zirconia-based ceramics,<sup>[12]</sup> and toughened steel alloys.<sup>[13]</sup> In contrast to these specific families of materials, the toughening and strengthening strategies evolved in natural composites are less dependent on the chemistry of the constituent phases and therefore can potentially be implemented in a wider range of material classes.<sup>[6]</sup> Such independence on the specific chemistry of the system opens the possibility of potentially incorporating important additional functionalities, such as bioresorbability, self-healing, recyclability, and regeneration.

Intrinsic and extrinsic toughening mechanisms have been implemented in synthetic materials using a variety of processing techniques such as layer-by-layer deposition,<sup>[14]</sup> ice-templating,<sup>[15]</sup> lamination approaches,<sup>[16]</sup> laser patterning,<sup>[17]</sup> magnetic alignment technologies,<sup>[18]</sup> and 3D printing.<sup>[19]</sup> Lamination of ceramic layers with thicknesses in the range 10–500  $\mu\text{m}$  is a well-known strategy to increase the fracture toughness of brittle materials through crack deflection and delamination mechanisms.<sup>[20]</sup> Such extrinsic mechanisms have also been successfully implemented at length scales down to 1  $\mu\text{m}$  and 200 nm using brick-and-mortar scaffolds produced by ice-templating or magnetic alignment of inorganic platelets, respectively. More recently, the formation of nanoscale mineral bridges interconnecting inorganic platelets was shown to be an effective intrinsic mechanism to increase the strength of brick-and-mortar nacre-like composites.<sup>[18b,21]</sup> These developments have now led to a rich palette of possible processing technologies for the fabrication of strong and tough lightweight composites that capture some of the design principles found in biological materials. To translate these new materials into a broad range of industrial applications, it is essential to identify and further develop processing routes that are sufficiently robust for the fabrication of bioinspired composites at larger length scales in a manner that they may be integrated into macroscopic structures. These technologies should enable independent control over the toughening mechanisms at multiple length scales in order to design bioinspired architectures that best fulfill the mechanical demands of the chosen application. Finally, control over such multiscale toughening mechanisms requires a quantitative understanding of the structure-property relationships that govern the mechanical performance of the resulting composite material.

Here, we design and study nacre-like composites that combine intrinsic and extrinsic mechanisms at multiple length scales to achieve high strength and toughness using upscalable and robust processing routes. Their high strength results from the intrinsic toughening achieved by a brick-and-mortar structure interconnected by mineral bridges at the nanoscale. These structures are combined with thick polymer lamella to form multilayered brittle-ductile laminates featuring extrinsic toughening mechanisms at the microscale. The mechanical properties of laminates made with different types of polymers and layer thicknesses are investigated to shed light on the structure-property relationships of these bioinspired composites. Our experimental findings are interpreted using simple fracture mechanics arguments to establish design criteria for

the fabrication of multiscale laminates with high stiffness, strength, and toughness. Since our composite laminates resemble the multiscale architecture of mollusk shells, this study also sheds light onto the possible role of the organic mesolayers that separate the brick-and-mortar structure of nacreous layers grown during seasonal fluctuations.

## 2. Results and Discussion

Biologically inspired multiscale composites were fabricated by combining two processing routes (**Figure 1A–D**). First, a vacuum-assisted magnetic alignment (VAMA)<sup>[21a]</sup> technique followed by hot pressing was used to prepare brick-and-mortar architectures consisting of interconnected alumina platelets<sup>[23]</sup> of thin lamellar architecture that were separated by graphite paper. In a second step, layers of this brick-and-mortar structure were separated while carefully preserving their structure and the graphite paper was removed. Third, the ceramic scaffolds were restacked, layered with polymer films or frames of controlled thicknesses, infiltrated with an epoxy matrix, and cured to result in multiscale laminates with alternating brittle and ductile layers of varying thickness and material composition. Because of imperfections on the surface of the ceramic scaffolds, a minimum distance of 70  $\mu\text{m}$  was always present when the scaffolds were restacked. Therefore, the spacing between brick-and-mortar layers is always filled with 70  $\mu\text{m}$  epoxy and a prescribed thickness of epoxy or polyetherimide (PEI).

Four different multiscale composite architectures were prepared and investigated in this work (**Figure 1E,F**). At smaller length scales, the composite displays the brick-and-mortar arrangement of interconnected alumina platelets that is infiltrated with either the stiffer (D230) or the softer (D400) crosslinked epoxy. At larger length scales, this brick-and-mortar layer is separated by the stiffer epoxy, the softer epoxy, or the tough polyetherimide layers to form laminates with a total of 13 layers. A specific nomenclature is used to easily identify these different multiscale architectures. Taking the composition “D230 +  $x$   $\mu\text{m}$  PEI” as an example, “D230” refers to the epoxy used as the polymer matrix at the smaller length scale (light grey in **Figure 1**) whereas “ $x$   $\mu\text{m}$  PEI” indicates the thickness and the type of polymer interlayer used in between the brick-and-mortar layers at larger length scales (yellow in **Figure 1**).

Polymers with very different mechanical properties were chosen as the organic phase at these distinct length scales in order to explore a broad design space and cover a wide range of possible fracture behaviors (**Figure 1E**). Mechanical characterization of these polymers and of the brick-and-mortar layers were performed to assess the deformation and fracture characteristics of these individual constituents separately (**Figure 1G–I**). Tensile mechanical tests reveal that the stiffer epoxy shows elastic modulus ( $E$ ) and fracture strength ( $\sigma_f$ ) of  $2.44 \pm 0.24$  GPa and  $63.18 \pm 3.7$  MPa, respectively. This is 20% higher than the modulus and strength values obtained for the softer epoxy. As a result of this higher stiffness and strength, the stiffer epoxy yields at a strain (5.6%) that is  $\approx 20\%$  lower than that of the softer polymer (6.8%). In contrast to these relatively weak crosslinked thermosets, the PEI polymer used at the laminate scale exhibits a higher yield strength of  $105 \pm 1.9$  MPa while maintaining a comparable elastic modulus of  $2.46 \pm 0.04$  GPa.

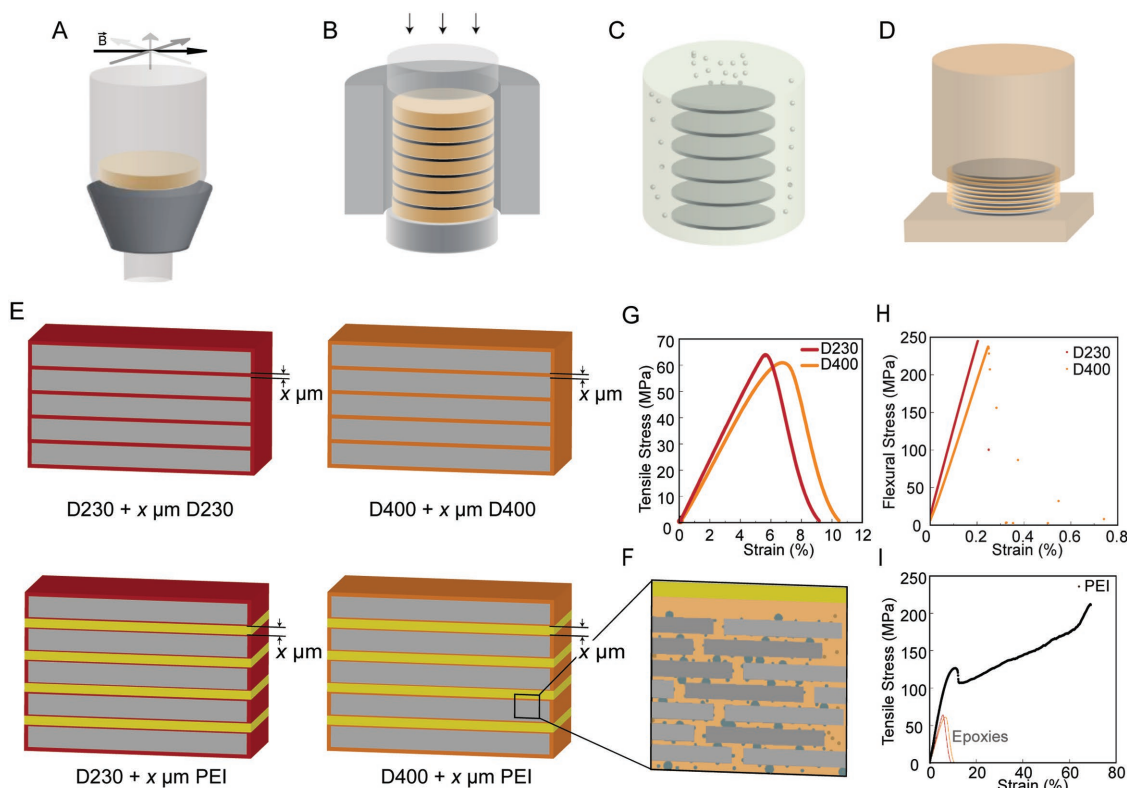


**Figure 1.** Fabrication process of multilayered nacre-like composites and mechanical properties of the individual layers. A) Magnetically functionalized alumina platelets suspended in water are aligned by rotating magnetic fields and consolidated into green bodies using a vacuum assisted magnetic alignment process.<sup>[21a]</sup> B) Scaffold green bodies (brown) are layered with graphitic paper spacers (dark grey) in a graphite die before sintering under pressure, to produce thin layered ceramic scaffolds. The ceramic scaffolds (light grey) are C) separated to remove the graphite spacers, D) replacing them by films or frames of PEI (light brown). These multilayered composites are infiltrated with epoxy and cured between copper blocks. E) Multiscale composite architectures are fabricated from epoxy or a combination of epoxy and PEI using this process. F) The resulting composites exhibit three levels of hierarchy: a brick-and-mortar ceramic microstructure with nanoscale mineral bridges networking the platelets together, further structured by laminating with additional polymer on the millimeter scale. G) Bulk tensile properties of the DGEBA epoxies cured with either 230 or 400 g mol<sup>-1</sup> polypropylene oxide diamine, which were used as polymer matrix at smaller length scales and interlayers in some of the laminates. H) Flexural properties of the brick-and-mortar layers infiltrated with the two different epoxies. I) Bulk tensile properties of the tough thermoplastic polymer PEI used as interlayers in some of the laminates at larger length scales.

Most importantly, extensive plastic deformation is observed for the PEI polymer, as demonstrated by a very high strain-at-rupture of 72% (Figure 1I).

Flexural tests on bulk brick-and-mortar samples containing either the softer or the stiffer epoxy show that these layers exhibit comparable elastic modulus and fracture strength. Values for  $E$  and  $\sigma_f$  of respectively  $101.4 \pm 6.6$  GPa and  $241.2 \pm 7.6$  MPa were measured for specimens infiltrated with the softer epoxy, whereas samples containing the stiffer epoxy showed  $E = 102.3 \pm 9.9$  GPa and  $\sigma_f = 234.1 \pm 20.5$  MPa. Using notched samples, we also observed that both bulk brick-and-mortar composites show similar fracture toughness ( $K_{IC}$ ) in the range 5–6 MPa m<sup>1/2</sup> with a gradual decrease in load bearing capacity beyond the peak load (Figure S2, Supporting Information). The measured  $K_{IC}$  values are roughly double than that of pure alumina,<sup>[22]</sup> which reflects the intrinsic toughening mechanism arising from the interconnected alumina platelets at the nanoscale.<sup>[21a]</sup> The ability to carry load beyond the peak indicates that the brick-and-mortar structure also exhibits some level of extrinsic toughening that prevents catastrophic failure of the material.<sup>[23]</sup>

The combined effect of the intrinsic toughening provided by the brick-and-mortar layers and the strong extrinsic toughening expected from the laminate structure was investigated by measuring the mechanical response of specimens with varying thickness ( $x$ ) of the laminate polymer layers (Figure 2). Unnotched samples were characterized in terms of elastic modulus ( $E$ ) and fracture strength ( $\sigma_{f,c}$ ), whereas notched beams were used to record the stress intensity factor ( $K_I$ ) on the sample as a function of the imposed load-line displacement.

Our results show that an increase in the thickness of the polymer interlayers enhances significantly the energy dissipation during fracture if the softer epoxy or the PEI polymers are used (Figure 2A–D). Such increase in fracture energy is evidenced by the increasing area under the  $K_I$  versus displacement curves. Notably, this toughening effect occurs without a major drop in the elastic modulus, fracture strength, and maximum stress intensity factor ( $K_{I,max}$ ) of the composite (Figure 2E–H). The arrangement of layers parallel to the loading direction (Voigt configuration) ensures that the total deformation of the laminate is dominated by the stiff layer, leading to a small variation in  $E$  and  $\sigma_{f,c}$  as the polymer layer thickness is increased.

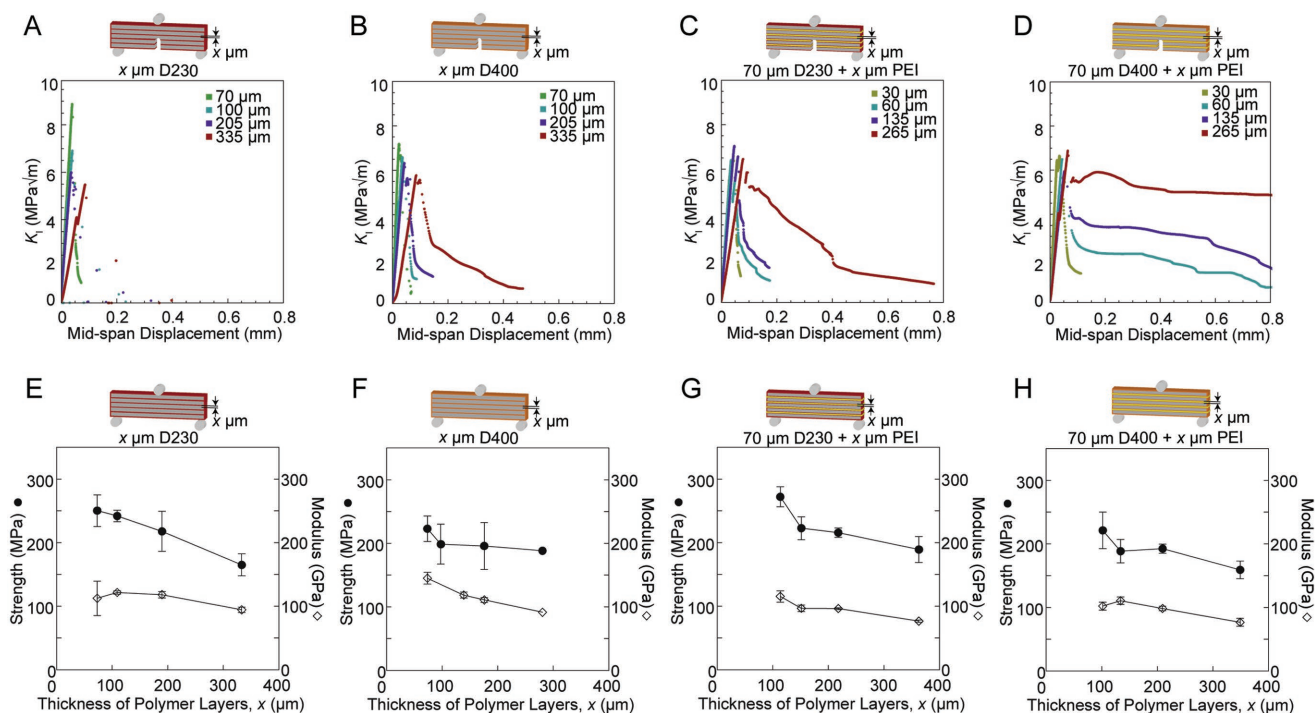


**Figure 2.** Mechanical characterization of composite laminates. Representative single edge notched bending (SENB) curves A–D) and flexural data E–H) for the four multiscale composite architectures as a function of the interlayer thickness. Polypropylene diamines of 230 and 400 g mol<sup>−1</sup> were used as the polymer matrix of the brick-and-mortar layers shown in (A,E,C,G) and (B,F,D,H), respectively. PEI interlayers of increasing thickness were used in (C,D,G,H), whereas epoxy interlayers with 230 and 400 g mol<sup>−1</sup> hardeners were utilized in (A,E) and (B,F), respectively.

In contrast to the toughening effect observed for the softer epoxy and the PEI polymers, composites containing the stiffer epoxy as interlayers exhibited a stronger decay in load-bearing capacity for all the thicknesses tested and showed a noticeable decrease in  $K_{I,max}$  for increasing layer thicknesses.

To shed light on the origin of these distinct fracture behaviors and establish a more quantitative criterion for the toughening effect induced by the polymer interlayers, we examined the fracture profile of two typical specimens: a brittle sample that failed more abruptly and a toughened laminate that showed high energy dissipation during fracture (Figure 3A,B). The fracture profiles and corresponding load displacement curves are remarkably different. Despite the tortuous fracture path within the brick-and-mortar layers, cracks propagating in the more brittle laminate grow straight through most of the polymer interlayer resulting in lower energy absorption. By contrast, fracture of the toughened laminate is followed by extensive deformation of the polymer interlayers that bridge the two sides of the main crack, increasing significantly the fracture energy. Introducing a lamellar structure toughened with PEI interlayers, we observe that the plastic work of fracture increases to values as high as  $13 \pm 2$  kJ m<sup>−2</sup>, more than a 30-fold increase of the work of fracture compared to bulk brick-and-mortar composites of the same bulk polymer matrix ( $\approx 0.36$  kJ m<sup>−2</sup>).

We hypothesize that these remarkably different fracture mechanisms are governed by a balance between the elastic strain energy accumulated within the more brittle brick-and-mortar layer ( $U_b$ ) and the plastic energy that can be dissipated in the following ductile polymer interlayer ( $U_d$ ). According to

this interpretation, cracks propagating in the brittle layer can only be arrested by the polymer layer if  $U_d > U_b$ . If this condition is satisfied, the initially fast-propagating crack will be arrested within the ductile polymer layer. This should allow for extensive plastic deformation of the undamaged remaining ductile layer, thus enhancing the toughness of the laminate. To test this hypothesis, we evaluate the effect of the energy ratio  $U_d/U_b$  on the toughness of all the investigated specimens (Figure 3C). The energy ratio per unit width is equivalent to  $(G_{IC,d}t_d)/(G_{IC,b}t_b)$ , where  $G_{IC,b}$  and  $G_{IC,d}$  are the strain energy release rates and  $t_b$  and  $t_d$  are the thicknesses of the brittle and ductile layers, respectively (Table S1, Supporting Information). We note that this energy balance is based purely on the elastic term of the strain energy release rate ( $G_{IC}$ ), since plastic energy dissipation is not expected within the layers at the very high crack propagation speeds at fracture initiation. Using the work of fracture to quantify the toughness of the laminate, we observe that significant toughening is indeed only achieved if the criterion  $\frac{G_{IC,d}t_d}{G_{IC,b}t_b} > 1$  is satisfied (Figure 3C). This energy ratio

provides, therefore, a simple and straightforward minimum requirement for the design of toughened laminates based on the fracture energies of the constituent brittle and ductile phases.

While composites that meet this requirement will not fail abruptly after fracture initiation, how much load laminates can continue to bear is a function of how stresses are transferred to the polymer interlayer. We observed that the polymer matrix within the brick-and-mortar structure plays an important role



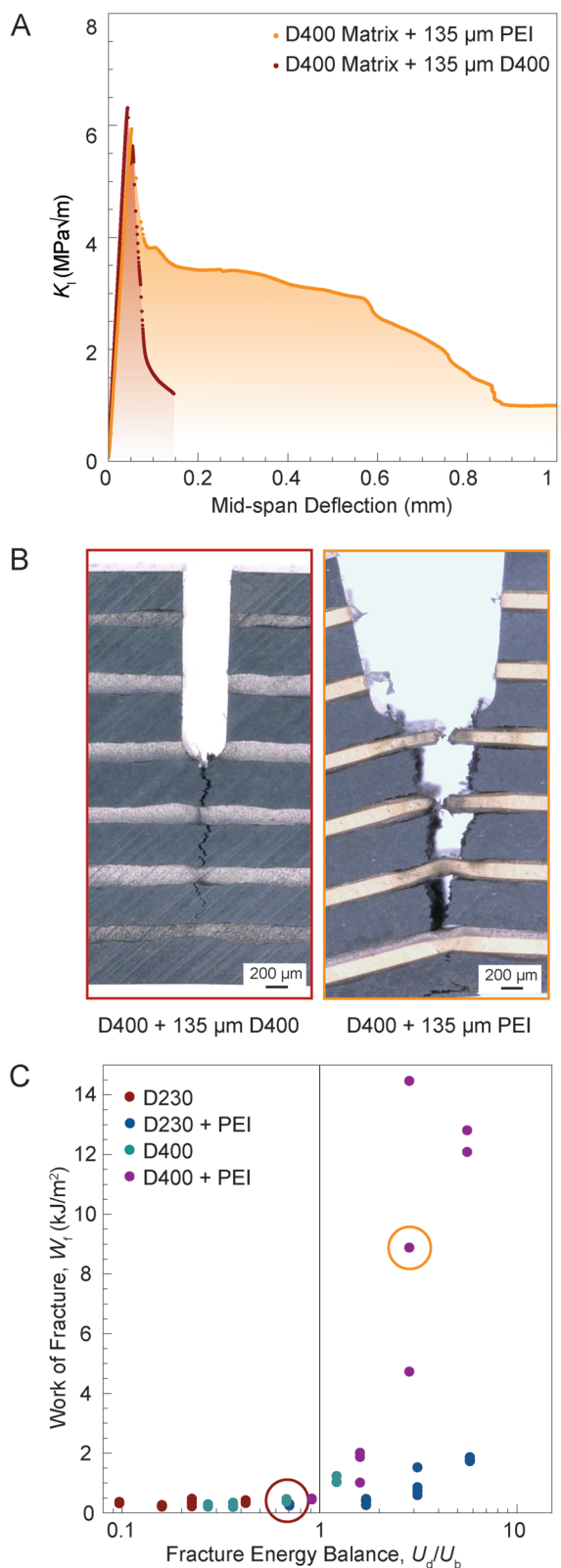


**Figure 3.** Work of fracture of multiscale composite laminates is strongly affected by a simple energy balance. A) Representative single edge notched bending curves of laminates that satisfy (orange) or not (red) the energy criterion for plastic deformation of the polymer interlayer. The

in the energy absorption by the polymer interlayer after the main crack has propagated through the brittle layers. The softer polymer matrix (D400) allows for higher energy dissipation in the PEI interlayer as compared to the stiffer epoxy (D230). This might result from several factors at play during fracture of the laminate. First, the thin layer of epoxy always present on the surface of the brick-and-mortar layers is expected to absorb part of the kinetic energy of the fast-propagating crack. Given that the softer epoxy (D400) has a nearly threefold higher fracture toughness ( $G_{IC}$ , Table S1, Supporting Information) than the stiffer epoxy (D230), it is expected to have a protective effect on the PEI interlayer, preserving a thicker PEI ligament (Equation (S1), Supporting Information) that maintains more capacity to bear load during failure (Figure 3A,B). Second, the more extensible nature of the epoxy crosslinked with the D400 amine facilitates shear deformation at the interface with the brittle layer when only the polymer interlayers connect the laminate surfaces. Such shear deformation close to the brittle layer interface is essential for the creation of bridging ligaments that dissipate further energy during fracture (Figure S3, Supporting Information).

Once a criterion for extrinsic toughening has been established, we now focus on the quantification of the fracture energy of laminates that satisfy this criterion. A more quantitative analysis of the fracture behavior of specimens containing the softer epoxy (D400) as the polymer matrix and the thermoplastic PEI as the polymer interlayer allows us to gain more insights into the key parameters controlling the multiscale toughening mechanisms of our hierarchical nacre-like composites.

The mechanical response (Figure 2D) and the fracture profile (Figure 3B) of these specimens indicate that intrinsic and extrinsic toughening mechanisms contribute to the resistance of the structure against crack initiation and propagation, respectively (Figure 4). Despite some level of extrinsic toughening,<sup>[23]</sup> the interconnected brick-and-mortar architecture acts predominantly ahead of the crack tip to enhance the crack initiation resistance beyond the values expected from the inorganic and organic constituent phases alone. This is reflected in the  $K_{IC}$  in the range 5–6 MPa m<sup>1/2</sup> measured for the brick-and-mortar structure,<sup>[21a]</sup> which is significantly higher than the value around 3 MPa m<sup>1/2</sup> typically observed for alumina.<sup>[22]</sup> We quantify the role of this intrinsic toughening mechanism on the fracture resistance of the composite laminates by estimating the effect of the polymer layer thickness on the stress intensity factor required for the nucleation of a crack in the brittle phase ( $K_{IN}$ ).<sup>[24]</sup> Assuming that the brittle brick-and-mortar structure dominates the elastic fracture energy of the laminate ( $J_e$ ), we estimate the  $K_{IN}$  values of specimens with increasing polymer layer thicknesses from the peak load of the flexural

difference in mechanical performance between laminates with the distinct polymer interlayers is highlighted by difference in areas under the curves. B) Cracks initiated in samples that do not fulfill the energy criterion pass through interlayers with little evidence of toughening, whereas the laminates that satisfy the criterion show extensive plastic deformation of the polymer interlayers. C) The work of fracture for all the investigated laminates, plotted as a function of the fracture energy ratio, shows that toughness improvement can only occur if the proposed energy criterion is satisfied.

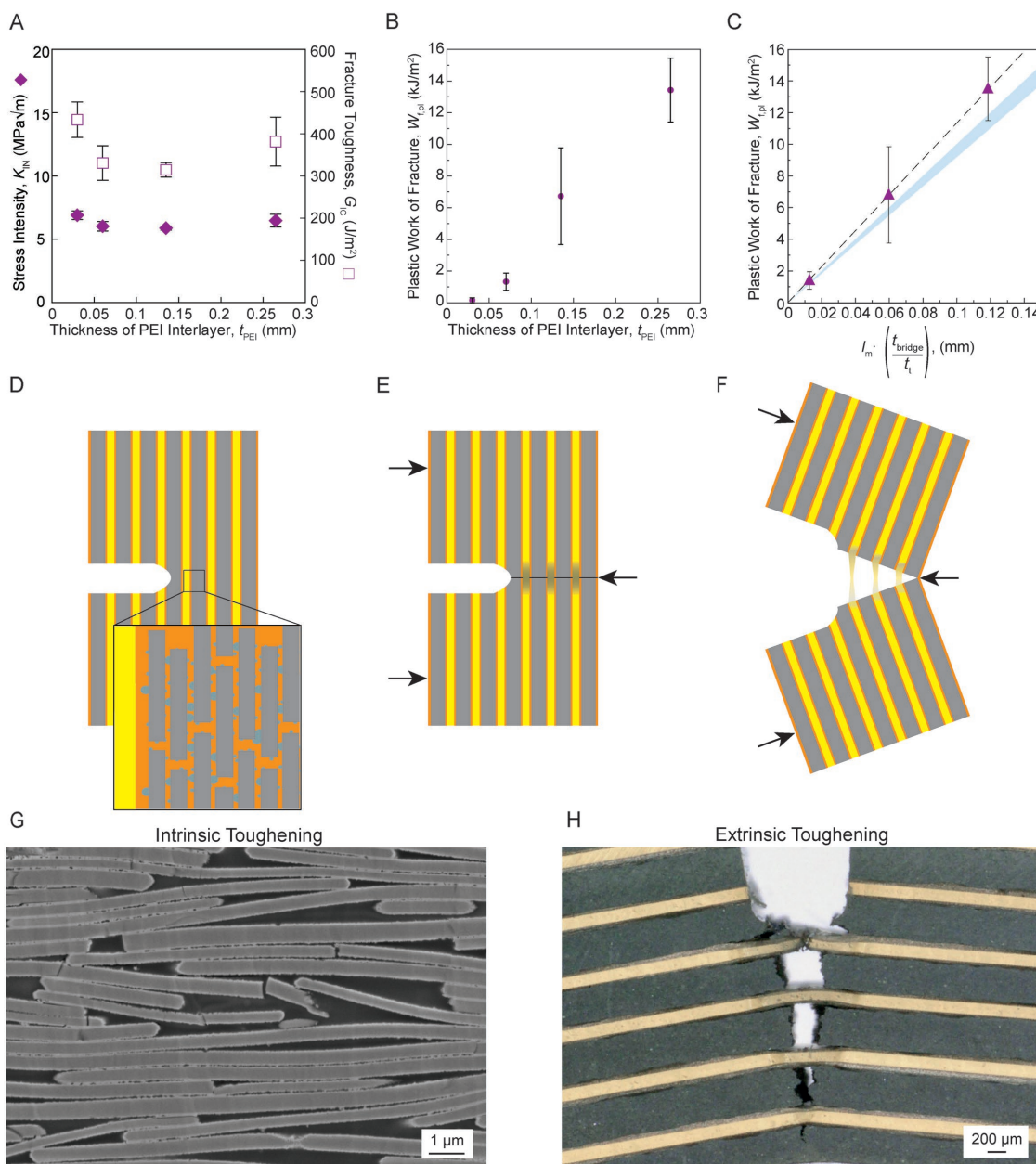


**Figure 4.** Quantification of intrinsic and extrinsic toughening mechanisms at play during fracture of the nacre-like multiscale composite laminates. A) At crack initiation, the stress intensity factor,  $K_{IC}$ , and the fracture toughness,  $G_{IC}$ , are effectively constant (within error) regardless of PEI interlayer thickness. B) Plastic work of fracture increases with increasing PEI interlayer thickness. C) Linear correlation between the plastic work of fracture and the normalized PEI bridge thickness when corrected for damage introduced during crack arresting. Values predicted from the measured modulus of toughness for PEI ( $\Phi_{PEI}$ ) are shown in blue. D) Multiscale structure of the pristine laminate. E) Brittle brick-and-mortar layers all fracture at very low deformations. F) Polymer interlayers are sheared at the brittle–ductile interface before forming bridging ligaments that undergo necking under tensile stresses. The polymer layers (ligaments) bridge the crack and prevent composite failure, even after significant deformation of the laminate. G) Brick-and-mortar composite layers provide intrinsic toughening mainly through mineral bridges between platelets. H) Laminate after complete fracture showing evidence of extrinsic toughening by polymer (ligament) bridging.

tests using linear elastic fracture mechanics. Interestingly, the  $K_{IN}$  of such laminates was found to be independent of the thickness of the polymer interlayer (Figure 4A).

In previous work on metal–ceramic laminates, this critical stress intensity factor ( $K_{IN}$ ) was shown to increase with the thickness of the ductile metal layer.<sup>[24]</sup> This toughening effect is explained by the fact that the metal layer of such laminates

is able to store a large portion of the elastic energy concentrated at the tip of the crack, reducing the actual stress intensity factor ( $K_I$ ) experienced by the brittle ceramic layer that is further away from the crack tip. The lower stress concentration at the ceramic layer requires that a higher  $K_I$  is applied to initiate fracture in the brittle phase of the laminate. However, such an effect is only observed if ductile and brittle layers show

comparable elastic modulus.<sup>[25]</sup> This condition is not satisfied by our composite laminates, since the polymer is two orders of magnitude softer than the ceramic phase. Given such a high elastic modulus contrast, the possibility to introduce a polymer layer that can increase the energy dissipation through plastic deformation without compromising the  $K_{IN}$  of the composite is a major asset for the design of our laminates.

Plastic deformation of the polymer phase behind the main crack is the major extrinsic toughening mechanism of our composite laminates. The contribution of this mechanism to the total toughness of the composites was estimated by calculating the plastic component of the measured total work of fracture ( $W_{f,pl}$ ). Our estimations show that the plastic work of fracture increases linearly with the thickness of the polymer interlayer (Figure 4B). This effect can be interpreted on the basis of the mechanism of energy dissipation that takes place within the polymer phase as a crack propagates through the lamellae. Because the brick-and-mortar brittle layers have significantly lower failure strain than the polymer interlayers, fracture of the successive brittle layers occurs almost immediately one after the other when the bending load is applied across the layered structure. This results in a multilayered material where all the brick-and-mortar layers have failed (Figure 4D), but the polymer interlayers remain intact and are able to form bridging layers (ligaments) between the cracked surfaces as the flexural test continues (Figure 4E). After fracture of the brittle ceramic layers, the elastic energy stored in the material is transferred to the ductile polymer layers by shear stresses developed at the brittle/ductile interfaces.<sup>[26]</sup> Using a simple shear lag model, one can show that such shear stresses extend up to a maximum length along the interface ( $l_m$ ) that is comparable to the thickness of the ceramic-like brittle layer ( $t_b$ ).<sup>[24]</sup> This prediction was confirmed by optical microscopy images of the laminates after fracture, where the region of sheared polymer is clearly identified by changes in local brightness throughout the polymer interlayer (Figure S4, Supporting Information). Shearing of the polymer adjacent to the ceramic surface eventually leads to partial debonding of the polymer interlayer. These effects lead to the formation of polymer bridges (ligaments) between the laminate surfaces.

Such polymer bridges exert a crack closing traction that counteracts the externally applied tensile stresses. Complete opening of the crack is only possible if the polymer bridges are totally deformed by necking followed by fracture under the locally imposed tensile stresses (Figure 4F). Assuming that the plastic energy dissipated in the composite arises predominantly from the deformation of the bridging polymer layers in pure tension, one would expect the work of fracture  $W_{f,pl}$  to increase linearly with the relative thickness of the ductile polymer bridge layer ( $t_{bridge}/t_t$ ), following the relation

$$W_{f,pl} = l_m \Phi (t_{bridge} / t_t) \quad (1)$$

where  $t_t$  is the sum of thicknesses of the brittle and ductile layers,  $l_m$  is the maximum shear length, and  $\Phi$  is the energy per unit volume consumed during stretching of the polymer layer until failure. It is important to highlight the direct proportionality between the work of fracture and the stress transfer length  $l_m$ , which arises from the shear lag model explained above. In this description, the dimension 2  $l_m$  sets the length of the

polymer bridge that needs to be fully deformed under tension in order to completely separate the two laminate surfaces. In this context, extensive shearing of the polymer at the interface with the brittle layer is essential to generate long polymer bridges that absorb high amounts of energy during fracture.

We note that the thickness of the polymer bridge layer ( $t_{bridge}$ ) is equivalent to the ductile polymer interlayer thickness ( $t_d$ ) corrected for an effective damage length  $\delta$  generated during arresting of the fast-propagating crack within the polymer layer:  $t_{bridge} = t_d - \delta$ . Using a simple energy balance, we estimate such an effective damage length to lie between 33 and 40  $\mu\text{m}$  for all the investigated composite laminates (see the Supporting Information). Using  $\delta$  values estimated through this energy criterion (Table S2, Supporting Information), one can plot the experimentally measured plastic work of fracture against the term  $l_m(t_{bridge}/t_t)$  of Equation (1) (Figure 4C). From the slope of the linear dependence between  $W_{f,pl}$  and  $l_m(t_{bridge}/t_t)$ , we predict a  $\Phi$  value of 112  $\text{MJ m}^{-3}$  for the PEI layers used in our laminates. Remarkably, this value is in close agreement with the modulus of toughness,  $\Phi_{PEI}$ , in the range 92–99  $\text{MJ m}^{-3}$  obtained from independent tensile experiments on bulk PEI samples (Figure 1H and Figure S1, Supporting Information). Thus, our quantitative analysis effectively captures the toughening mechanisms that control the fracture behavior of the investigated laminates (Figure 4) in the crosslayer direction.

As with other traditional composite laminates, these materials have highly anisotropic stiffness and strength, which can reduce their functionality when stresses are applied in the third through-thickness direction. However, unlike traditional composites, the presented hierarchical nacre-like composites are 2D isotropic in plane, thereby eliminating the weak transverse axis of fiber-reinforced materials. When appropriately oriented for stress in the in-plane direction, this structure produces laminates with enhanced fracture toughness without major compromise to stiffness and strength as would be the case for orthotropic ply stacking of traditional composites.

In addition to its remarkable combination of mechanical properties, our nacre-like hierarchical composites provide, for the first time, a model synthetic system structured at three hierarchical levels comparable to the length scales of mollusk shells. If combined with computer simulation studies and advanced characterization of biological species, such a model system offers a unique experimental platform for a systematic investigation of the multiscale design principles of biological shells.

Because it exhibits polymer chemistry and length scales comparable to those of conventional fiber-reinforced polymers, the reported nacre-like hierarchical composites can potentially be directly implemented in materials already used in structural applications. The high toughness, strength, and stiffness of these bioinspired materials could be readily utilized, for example, as protective layers in turbine blades or in the leading edge of aircraft foils to locally minimize abrasion, impact damage, and wear of these important structural components. Alternatively, the chemistry of the inorganic and organic phases could be adapted to create resorbable and osteo-inductive nacre-like hierarchical materials for bone regeneration applications. This could potentially address the lack of bone replacement materials that combine bioresorbability with high stiffness and fracture toughness.

### 3. Conclusions

Nacre-like composites with superimposed hierarchical toughening effects can be fabricated if a brittle–ductile laminate architecture at the macroscale is combined with a brick-and-mortar arrangement of interconnected mineral phases at the nanoscale. In this hierarchical design, the interconnected brick-and-mortar morphology provides an intrinsic toughening mechanism that increases the initial strength of the composite, whereas the brittle–ductile laminated structure generates extrinsic toughening effects that enhance the energy dissipation during fracture. Extrinsic toughening arises from the ductile deformation of the polymer layers of the laminate behind the main crack tip. For this mechanism to be activated, the fracture energy of the polymer lamella should exceed the elastic energy stored within the stiffer brick-and-mortar lamella at failure. Multiscale composites that satisfy this energy criterion show a linear increase in dissipative fracture energy as the polymer layer of the laminate increases in thickness. This linear dependence can be rationalized in terms of the energy dissipated within the polymer layers bridging the fractured brittle lamella after the main crack has propagated through the laminate. Importantly, this highly dissipative process is achieved without compromising the high toughness of the composite against crack initiation, which remains constant irrespective of the polymer layer thickness. The ability to combine strength and toughness through the hierarchical organization of organic and inorganic building blocks effectively captures a major design principle of strong and tough biological composites, such as nacre, teeth, and bone. Taken as a model system, our hierarchical synthetic composites might help elucidate, in future studies, the possible mechanical role of the sub-millimeter organic mesolayers created under seasonal fluctuations in the nacreous layer of mollusk shells.

### 4. Experimental Section

**Composite Fabrication:** Dry magnetized platelets (2 g, 12.5 vol%) were produced as detailed by Grossman et al.<sup>[21a]</sup> and suspended in a 4 mL solution of 2% polyvinyl alcohol ( $M_w = 30\text{--}70$  kDa, Sigma-Aldrich, Germany) and 0.07% of poly acrylic acid ( $M_w = 8$  kDa, Polysciences, USA). Ceramic scaffolds were cast using a vacuum assisted magnetic alignment setup by pulling 100 mbar vacuum for 1 min. The resulting disc-shaped compacts with diameter of 46 mm (Figure 1A) were dried overnight. Dry compacts were subsequently debound in air (500 °C, 3 h) and stacked in a 50 mm graphite die, separated by discs of graphite paper (Figure 1B) before spark plasma sintering under nitrogen. Sintering was carried out at 800 °C under an external pressure of 40 kN. Samples were heated at a rate of 50 °C min<sup>−1</sup> and kept for 45 min at this maximum temperature and pressure (water cooling FCT Systeme GmbH, Germany) to produce a stack of 400 µm thick ceramic discs of close matching surfaces. Other disc thicknesses can be produced by casting larger quantities of platelet suspension. The density, stiffness, and strength of these ceramic disks can be modulated through variation of sintering temperature and pressure, as described in Grossman et al.<sup>[23]</sup> Any irregularity in edge thickness was removed by polishing with SiC paper. Discs were separated after a brief soak in water, facilitating spontaneous removal of graphite paper spacers, and then restacked, resulting in close matching surfaces between neighboring samples. Ceramic discs were dried at 100 °C overnight before layering with discs of commercially available polyetherimide resin films (PEI, Ultem 1000, CS Hyde, USA) or ring-shaped frames punched from them to

control the thickness of the epoxy interlayers. The multilayered stacks of alternating ceramic and polymer layers were then infiltrated with a stoichiometric mixture of diglycidyl ether bisphenol A (DGEBA, Araldite GY 250, Huntsman, Belgium) and polypropylene oxide diamine with a molecular weight of 230 or 400 g mol<sup>−1</sup> (Jeffamine D230 or Jeffamine D400, Huntsman, Belgium) by degassing submerged samples in a desiccator for 45 min (Figure 1C). The use of crosslinkers Jeffamine D230 and Jeffamine D400 led to stiffer and softer epoxies, respectively, due to different crosslink densities. These epoxies are indicated throughout the text as simply D230 and D400. Infiltrated samples were subsequently cured between copper blocks for 2 h at 80 °C followed by a postcure at 135 °C for 3 h (Figure 1D). Bulk samples were infiltrated by isostatic pressure (KIP 100E, P.O. Weber, Germany) as detailed by Grossman et al.<sup>[21a]</sup>

**Characterization:** Flexural tests were performed using a universal testing machine (Autograph AGS-X, Shimadzu, Japan) on specimens that were cut and polished to  $S = 20\text{ mm} \times w = 2\text{ mm} \times b = 1.5\text{ mm}$  and  $S = 40\text{ mm} \times w = 4\text{ mm} \times b = 3\text{ mm}$  for bulk and multilayered samples respectively, as specified in ASTM designation C1161-13. Single edge notched bending tests were performed on specimens (with thickness  $b$ ) cut and polished to  $4b \times b/2 \times b$  with a  $b/2$  deep razor and polishing paste sharpened notch, perpendicular to the plane of platelet alignment, as specified by ASTM designation D5045-99. Layer thicknesses were determined by image analysis of high contrast light micrographs (Wild M10, Leica, Germany) using the FIJI software package.<sup>[27]</sup> The elastic modulus of D230/DGEBA and D400/DGEBA epoxies were measured by tensile tests using dog-bone shaped samples cast in molds  $S = 12\text{ mm} \times w = 1.75\text{ mm} \times b = 1.65\text{ mm}$ . The elastic modulus of PEI was measured by tensile tests of dog-bone shaped samples sized  $12\text{ mm} \times 2\text{ mm}$ , punched from 135 µm thick films.

### Supporting Information

Supporting Information is available from the Wiley Online Library or from the author.

### Acknowledgements

This work was carried out with financial support from the Swiss Competence Center for Energy Research (Capacity Area A3: Minimization of Energy Demand). The research also benefitted from support from the Swiss National Science Foundation within the framework of the National Center of Competence in Research for Bio-Inspired Materials and the SNF Project 200021\_156011. Dr. Kirill Feldman and Wilhelm Woigk are gratefully acknowledged for their help with experiments. The authors are also very thankful to Dr. Ambrose Taylor for the helpful discussions. Technical support from the Center for Optical and Electron microscopy of ETH Zürich (ScopeM) as well as the supply of Jeffamine and epoxy materials by Huntsman Advanced Materials (Switzerland) are also acknowledged.

### Conflict of Interest

The authors declare no conflict of interest.

### Keywords

bioinspired, composite materials, hierarchical structures, lightweight, toughness

Received: September 26, 2018

Revised: November 9, 2018

Published online: January 8, 2019



- [1] *On a European Strategy for Low-Emission Mobility*, European Union, Brussels, November **2017**, p. 13.
- [2] R. F. Gibson, *Compos. Struct.* **2010**, 92, 2793.
- [3] a) F. L. Matthews, R. D. Rawlings, *Composite Materials: Engineering and Science*, Chapman & Hall, London **1994**; b) S. Ramakrishna, J. Mayer, E. Wintermantel, K. W. Leong, *Compos. Sci. Technol.* **2001**, 61, 1189.
- [4] R. O. Ritchie, *Nat. Mater.* **2011**, 10, 817.
- [5] a) J. W. C. Dunlop, P. Fratzl, in *Annual Review of Materials Research*, Vol. 40 (Eds: D. R. Clarke, M. Ruhle, F. Zok), Palo Alto, **2010**, pp. 1–24; b) M. J. Buehler, *Nano Today* **2010**, 5, 379; c) P. Fratzl, *J. R. Soc., Interface* **2007**, 4, 637.
- [6] A. R. Studart, *Adv. Mater.* **2012**, 24, 5024.
- [7] P. Fratzl, R. Weinkamer, *Prog. Mater. Sci.* **2007**, 52, 1263.
- [8] R. O. Ritchie, *MRS Bull.* **2014**, 39, 880.
- [9] E. A. Zimmermann, E. Schaible, H. Bale, H. D. Barth, S. Y. Tang, P. Reichert, B. Busse, T. Alliston, J. W. Ager, R. O. Ritchie, *Proc. Natl. Acad. Sci. USA* **2011**, 108, 14416.
- [10] a) F. Barthelat, H. D. Espinosa, *Exp. Mech.* **2007**, 47, 311; b) F. Barthelat, C.-M. Li, C. Comi, H. D. Espinosa, *J. Mater. Res.* **2006**, 21, 1977; c) H. D. Espinosa, J. E. Rim, F. Barthelat, M. J. Buehler, *Prog. Mater. Sci.* **2009**, 54, 1059; d) M. I. Lopez, P. E. M. Martinez, M. A. Meyers, *Acta Biomater.* **2014**, 10, 2056; e) R. Z. Wang, H. S. Gupta, *Annu. Rev. Mater. Res.* **2011**, 41, 41.
- [11] M. D. Demetriou, M. E. Launey, G. Garrett, J. P. Schramm, D. C. Hofmann, W. L. Johnson, R. O. Ritchie, *Nat. Mater.* **2011**, 10, 123.
- [12] R. C. Garvie, R. H. Hannink, R. T. Pascoe, *Nature* **1975**, 258, 703.
- [13] A. Miserez, R. Muller, A. Rossoll, L. Weber, A. Mortensen, *Mater. Sci. Eng., A* **2004**, 387–389, 822.
- [14] L. J. Bonderer, A. R. Studart, L. J. Gauckler, *Science* **2008**, 319, 1069.
- [15] E. Munch, M. E. Launey, D. H. Alsem, E. Saiz, A. P. Tomsia, R. O. Ritchie, *Science* **2008**, 322, 1516.
- [16] G. Mayer, *Mater. Sci. Eng., C* **2006**, 26, 1261.
- [17] a) G. Bullegas, S. T. Pinho, S. Pimenta, *Compos. Sci. Technol.* **2016**, 131, 110; b) M. Mirkhalaf, A. K. Dastjerdi, F. Barthelat, *Nat. Commun.* **2014**, 5, 3166.
- [18] a) R. M. Erb, R. Libanori, N. Rothfuchs, A. R. Studart, *Science* **2012**, 335, 199; b) H. Le Ferrand, F. Bouville, T. P. Niebel, A. R. Studart, *Nat. Mater.* **2015**, 14, 1172.
- [19] a) G. X. Gu, F. Libonati, S. D. Wettermark, M. J. Buehler, *J. Mech. Behav. Biomed. Mater.* **2017**, 76, 135; b) G. Xiang Gu, I. Su, S. Sharma, J. L. Voros, Z. Qin, M. J. Buehler, *J. Biomech. Eng.* **2016**, 138, 021006.
- [20] a) F. D. Minatto, P. Milak, A. De Noni, D. Hotza, O. R. K. Montedo, *Adv. Appl. Ceram.* **2015**, 114, 127; b) M. E. Launey, E. Munch, D. H. Alsem, E. Saiz, A. P. Tomsia, R. O. Ritchie, *J. R. Soc., Interface* **2010**, 7, 741.
- [21] a) M. Grossman, F. Bouville, F. Erni, K. Masania, R. Libanori, A. R. Studart, *Adv. Mater.* **2017**, 29, 1605039; b) V. Naglieri, B. Gludovatz, A. P. Tomsia, R. O. Ritchie, *Acta Mater.* **2015**, 98, 141.
- [22] P. F. Becher, *J. Am. Ceram. Soc.* **1991**, 74, 255.
- [23] M. Grossman, F. Bouville, K. Masania, A. R. Studart, *Proc. Nat. Acad. Sci. USA* **2018**, 115, 12698.
- [24] H. C. Cao, A. G. Evans, *Acta Metall. Mater.* **1991**, 39, 2997.
- [25] M. C. Shaw, D. B. Marshall, M. S. Dadkhah, A. G. Evans, *Acta Metall. Mater.* **1993**, 41, 3311.
- [26] T. L. Anderson, *Fracture Mechanics Fundamentals and Applications*, Taylor & Francis, Boca Raton, FL **2005**.
- [27] a) J. Schindelin, I. Arganda-Carreras, E. Frise, V. Kaynig, M. Longair, T. Pietzsch, S. Preibisch, C. Rueden, S. Saalfeld, B. Schmid, J. Y. Tinevez, D. J. White, V. Hartenstein, K. Eliceiri, P. Tomancak, A. Cardona, *Nat.aaaa Methods* **2012**, 9, 676; b) S. Preibisch, S. Saalfeld, P. Tomancak, *Bioinformatics* **2009**, 25, 1463; c) R. Dougherty, K. H. Kunzelmann, *Microsc. Microanal.* **2007**, 13, 1678.